Ultra-Rapid Rates of Water Splitting for Biohydrogen Gas Production through in vitro Artificial Enzymatic Pathways

Journal:	*Energy & Environmental Science*
Manuscript ID	EE-ART-03-2018-000774.R1
Article Type:	Paper
Date Submitted by the Author:	01-May-2018
Complete List of Authors:	Kim, Eui-jin ; Virginia Tech, Biological Systems Engineering Kim, Jae-Eung; Virginia Tech, Biological Systems Engineering Zhang, Yi-Heng P.; Tianjin Institute of Industrial Biotechnology,

SCHOLARONE™
Manuscripts

Ultra-Rapid Rates of Water Splitting for Biohydrogen Gas Production through *in vitro* Artificial Enzymatic Pathways

Eui-Jin Kim,[1,†] Jae-Eung Kim,[1] and Yi-Heng P. Job Zhang [2] *

[1] Biological Systems Engineering Department, Virginia Tech, Blacksburg, Virginia 24061, USA

[2] Current address: Tianjin Institute of Industrial Biotechnology, Chinese Academy of Sciences, 32 West 7th Avenue, Tianjin Airport Economic Area, Tianjin 300308, China

[†] Current address: Department of Life Science and Basic Science Institute, Sogang University, Seoul 04107, Republic of Korea

Running title: Fastest Biohydrogen Production

* Corresponding Author: Y.-H. Zhang (ORCID ID: 0000-0002-4010-2250), email: yhjob_zhang@outlook.com, Tel: 001-540-235-4299.

Abstract

Unlocking the potential of the hydrogen economy requires breakthroughs of production, storage, distribution, and infrastructure. Here we demonstrate an *in vitro* artificial enzymatic pathway that can produce hydrogen at extremely high rates by splitting water energized by carbohydrates (e.g., starch). This fifteen hyperthermophilic enzymes pathway is comprised of ATP-free starch phosphorylation, an NAD-based pentose phosphate pathway, and a biomimetic electron transport chain consisting of a diaphorase, an electron mediator benzyl viologen (BV), and a [NiFe]-hydrogenase, whereas fast electron transfer was facilitated by utilizing a BV-conjugated diaphorase. The highest reaction rate of 530 mmol H_2/L/h was accomplished at 80°C. Two NAD-conjugated dehydrogenases were further applied to enable nine-day hydrogen production with a total turnover number of NAD of over 100,000, along with hyperthermophilic enzymes. This biohydrogen production system characterized in the highest chemical-energy efficiency and exceptionally-high reaction rate addresses challenges associated with cost-effective, distributed hydrogen production, off-board hydrogen storage, and infrastructure.

Keywords: biohydrogen, coenzyme engineering, electron transport chain, hydrogen economy, *in vitro* synthetic biology, water splitting,

Introduction

Hydrogen gas (H_2) is a clean energy carrier to likely replace fossil fuel-derived liquid fuels, due to higher energy conversion efficiencies, nearly zero pollutants to end users, and more energy storage density than rechargeable batteries [1,2]. Current thermochemical H_2 production means from fossil fuels are cost-competitive [3], but they cannot be scaled down due to the economy of scale [4]. The distributed H_2 is costly when transportation costs are included. It is highly expected that green, cost-competitive, distributed H_2 will be produced *via* water splitting powered by solar energy directly or indirectly [3,5-11]. Hydrogen production *via* high-speed water splitting may be energized by renewable carbohydrates (e.g., starch and biomass, a point energy source) with *in vitro* artificial enzymatic pathways [11-14] other than nonpoint energy sources (e.g., insolation with an average energy flux of ~200 W/m^2) [15], along with other benefits, such as low H_2 transportation costs, easy H_2 harvesting, and low capital expenditure of distributed H_2 generation bioreactors [4].

Microorganisms that naturally produce H_2 have evolved three major electron transport chains (ETCs) to do so. Photobiological H_2 production by microalgae is catalyzed by hydrogenase, which receives electrons from NADPH that is generated from photosystem I *via* the reduced ferredoxin catalyzed by ferredoxin-NADP$^+$ oxidoreductase (FNR) [16,17], but it suffers from very low volumetric productivity. Microbial dark fermentation rapidly converts glucose to pyruvate with the formation of either formate (for example, *Enterobacter* spp.) or reduced ferredoxin (for example, *Clostridium* spp.) as intermediate electron carriers [18], yielding two moles of H_2 per glucose. In *Clostridium* spp., another two moles of hydrogen per glucose can be produced from an NADH-dependent hydrogenase. This NADH-to-H_2 reaction, however, is thermodynamically unfavorable under the standard condition because the midpoint potential of H^+/H_2 redox couple ($E^0 = -414$ mV) is more negative than that of NADH ($E^{0'} = -320$ mV). This reaction occurs only under low hydrogen pressures [18]. However, some fermentative anaerobes have a so-called bifurcating hydrogenase [19] that couples the exergonic production of H_2 using reduced ferredoxin as the electron donor to the endergonic production of H_2 using NADH as the electron donor, allowing maximum H_2 production from glucose oxidation (i.e., four H_2 per glucose). Electron bifurcating enzymes are known to be widespread in anaerobic microbes [19]. As a result, the theoretical H_2 yields of dark fermentation are two or four H_2 per glucose, called the Thauer limit,

68   depending on the catabolic pathways and fermentation conditions [18, 20]. Although intensive

69   efforts in H_2-producing microorganisms by metabolic engineering and synthetic biology [18, 21],

70   they cannot break this limit due to the basic bioenergetics and thermodynamics of living

71   organisms.

72

73   *In vitro* enzymatic H_2 production systems have been demonstrated to split water energized by

74   carbohydrates and catalyzed by enzymatic pathways comprised of more than ten enzymes [11-14].

75   This approach is one of the most promising means for distributed H_2 production because it

76   achieves the theoretical yield of hydrogen generation, i.e., 12 moles of H_2 from one mole of

77   hexose along with water, with potentially-high volumetric productivities [2, 20]. Because

78   carbohydrates are produced through plant photosynthesis, this indirect water splitting energized

79   by carbohydrates is nearly carbon-neutral in terms of the whole life cycle. Recent efforts have

80   expanded the types of carbohydrates, such as, glycogen [13], starch [12], and biomass sugars [11]. These

81   efforts have also led to great increases in volumetric productivity [11], as well as decreases in

82   biocatalyst costs through utilization of thermostable enzymes with facile heat treatment

83   purification [22, 23], enzyme immobilization [24], and replacement of costly coenzymes [25-27].

84   However, these *in vitro* enzymatic pathways are based on prohibitively expensive and unstable

85   NADPH, which is generated from the pentose phosphate pathway (PPP). A major breakthrough

86   is urgently needed to replace NADP with the much more stable and less costly NAD [20, 26, 27], and

87   that was one of the goals of this study.

88

89   The first NAD-dependent enzymatic pathway that splits water for ultra-rapid hydrogen gas

90   production (**Fig. 1b**) was designed to replace the NADP-dependent PPP [11-14] (**Fig. 1a**).

91   Synergetic advances in non-fermentative pathway, coenzyme engineering, biomimetic NAD-

92   based ETC (**Fig. 1b**), and fast electron transfer between DI and BV (**Fig. 1c**), lead to ultra-rapid

93   volumetric productivity of over one gram of H_2 per liter per hour. Furthermore, the construction

94   of two NAD-conjugated dehydrogenases (**Fig. 1d**) extended the total turn-over number (TTN) of

95   NAD of more than 100,000 at 80°C.

96

NAD-Based PPP

The PPP generates two moles of NADPH from one mole of glucose 6-phosphate (G6P) using two dehydrogenases glucose 6-phosphate (G6PDH) and 6-phosphogluconate (6PGDH), respectively. The coenzyme preference of 6PGDH from *Thermotoga maritima* was rationally engineered to change its specificity from $NADP^+$ to NAD^+ [25]. To develop the first hyperthermophilic NAD-dependent PPP, we had to change the coenzyme preference of the *T. maritima* G6PDH from $NADP^+$ to NAD^+. An *in silico* homology model of *T. maritima* G6PDH was generated based on a G6PDH template of a mesophilic bacterium *Leuconostoc mesenteroides* (PDB: 1DPG, 35% identity). According to the three-dimensional structure of TmG6PDH with bound $NADP^+$ (**Fig. 2a**), key amino acid residues responsible for binding the 2′-phosphate group (S33, A64, and R65T66 positions) were altered by saturation mutagenesis. Three mutant libraries containing random mutations (NNK codons) at positions of 33, 64 or 65/66 were expressed in *E. coli* Top10 (**Fig. S1**). Three TmG6PDH mutant libraries were screened for their enhanced NAD^+-dependent activities based on the tetranitroblue tetrazolium double-layer screening method [28] (**Fig. S2**). There are several positive mutants for Libraries S33 and R65/T66 but no positive mutant for Library A64 (**Fig. 2b**). Positive colonies were re-screened (**Fig. 2b**) and the mutants exhibited highest activities were S33E and R65M/T66S. Finally, a combination of positive mutants resulted in the most active enzyme (mG6PDH -- S33E/R65M/T66S) (**Fig. 2b**). mG6PDH had a 30-fold decrease in its K_m on NAD^+ and had a 7.7-fold increase in its K_m on $NADP^+$ but no significant change in its k_{cat} value on NAD^+ (**Table S1**). The relative (NAD^+ *vs.* $NADP^+$) catalytic efficiency ratio (k_{cat}/K_m) of mG6PDH on NAD^+ and $NADP^+$ increased approximately 250-fold compared to that of wild-type G6PDH (**Table S1**). Thus, mG6PDH showed comparable coenzyme specificities for NAD^+ and $NADP^+$.

NAD-Based ETC

H_2 production *via* direct electron transfer from NADPH to H_2 is catalyzed by the NADP-specific soluble [NiFe]-hydrogenase (SHI) from *Pyrococcus furiosus*. A biomimetic ETC comprised of an NADPH rubredoxin oxidoreductase (NROR) from *P. furiosus,* which uses NADPH to reduce the abiotic electron mediator BV, was introduced to greatly improve H_2 production rates of SHI [12, 29]. When NAD^+ was used to replace $NADP^+$, a new transhydrogenase was needed to be discovered for rapidly catalyzing electron transfer from NADH to BV because $NADP^+$-

128   dependent NROR exhibits a very low activity on NAD^+ (**Fig. 3c**). The 3D-docking structure for

129   NROR with $NADP^+$ bound (**Fig. 3a**) suggested that the electrostatically positive-charged amino

130   acids (H165 and R166) of NROR could stabilize the binding with the 2′-phosphate of $NADP^+$.

131   Because diaphorase (DI) is a transhydrogenase that prefers NAD^+ to $NADP^+$ as an coenzyme [30],

132   an NAD^+-specific DI was searched from hyperthermophilic microorganisms. A new DI, which

133   was annotated as a probable nitrite reductase subunit (KEGG) in *T. maritima,* showed 53%

134   identity and 71% similarity with NROR. It has a negative-charged amino acid (E165) in the

135   nicotinamide cofactor binding site, suggesting its NAD^+ preference (**Fig. 3b**). The coenzyme

136   specificity of *T. maritima* DI for BV reduction was reversed compared to *P. furiosus* NROR (**Fig.**

137   **3c**).

138

139   An NAD^+-based ETC was designed to utilize three enzymes (i.e., mG6PDH, DI, and SHI) to

140   oxidize G6P and evolve H_2 with NAD^+ and BV as electron carriers (**Fig. 1b**). The proof-of-

141   concept experiments were conducted on 100 mM G6P at 50°C. In a negative control experiment

142   with a mixture of mG6PDH and SHI, a very low volumetric hydrogen productivity was observed

143   with a long lag period, whereas the maximum rate was 7 mmol H_2/L/h after three hours (**Fig.**

144   **3d**). With the addition of DI and BV, the maximum volumetric productivity increased by five-

145   fold to 36 mmol H_2/L/h (**Fig. 3d**). This result suggested that the first NAD-based biomimetic

146   ETC drastically increased volumetric productivity of H_2.

147

148   ## BV-Conjugated DI for Fast Electron Transfer

149   Inspired by natural spatially-organized complexes for facilitating rapid electron transfer among

150   adjacent enzymes, the BV-conjugated DI (called BCV-DI) was synthesized through benzyl (4-

151   carboxymethyl)benzyl viologen (BCV) with a cross-linking reagent 1-ethyl-3-(3-

152   dimethylaminopropyl)carbodiimide (**Fig. 4a**). The BV-conjugated DI led to an approximately

153   2.5-times higher $NAD(P)^+$-dependent BV reduction rate compared to that of a mixture of DI and

154   BV (**Table S2**). In the case of mG6PDH, DI, and SHI system on 100 mM G6P, the use of BV-

155   conjugated DI instead of DI and BV (**Fig. 1c**) doubled volumetric productivity to 67 mmol

156   H_2/L/h at 50°C compared to the BV-based ETC case (**Fig. 3d**). These results suggested increased

157   electron transfer between DI and BV in this conjugate.

158

159   The use of hyperthermophilic enzymes could have multiple benefits. These include 1) increasing

160   specific activities of enzymes, in particular SHI from the organism with the highest growth

161   temperature (e.g., 100°C for *P. furiosus*); 2) decreasing H_2 solubility in the aqueous reactants to

162   mitigate H_2 inhibition; 3) eliminating the chances of microbial contamination; and 4) decreasing

163   the viscosity of the aqueous solution for better mass transfer. An enzymatic hydrogen production

164   reaction with mG6PDH, SHI and BV-conjugated DI led to the peak volumetric productivity of

165   220 mmol H_2/L/h at 80°C (**Fig. 4b**). When NAD-preferred 6PGDH from *T. maritima* (m6PGDH)

166   [25] was added, the volumetric productivity increased to 370 mmol H_2/L/h. The addition of 6-

167   phosphoglucono-lactonase (6PGL) from *T. maritima* [31] further increased the volumetric

168   productivity to 450 mmol H_2/L/h (**Fig. 4b**).

169

170   ## Ultra-Rapid H_2 Production from Starch

171   This artificial enzymatic pathway (**Fig. 5a)** has four modules: 1) G6P generation from starch and

172   phosphate catalyzed by α-glucan phosphorylase followed by phosphoglucomutase (PGM); 2)

173   two moles of NADH are generated from one mole of G6P catalyzed by mG6PDH, 6PGL, and

174   m6PGDH *via* the NAD-based oxidative PPP; 3) H_2 production from NADH *via* the biomimetic

175   ETC containing BCV-DI and SHI; and 4) the regeneration of five moles of G6P from six moles

176   of ribulose 5-phosphate *via* the non-oxidative PPP and the partial gluconeogenesis pathway. As a

177   result, one mole of the anhydroglucose unit in the starch plus seven moles of water can produce

178   12 moles of H_2 and six moles of carbon dioxide (**equation 1**). In contrast to the previous starch-

179   to-H_2 pathways [12, 13], three major improvements have been made. They are: 1) the

180   demonstration of the first NAD-based PPP (**Fig. 5a**), 2) a biomimetic NAD-based ETC based on

181   a BCV-DI (**Fig. 1c**), and 3) the first set of fifteen hyperthermophilic enzymes that were stable at

182   80°C. Five hyperthermophilic enzymes (i.e., PGI [32], PGM [33], m6PGDH [25], mG6PDH (here), and

183   DI) were used for *in vitro* biohydrogen generation at 80°C (**Table 1).**

184         $$C_6H_{10}O_5 \text{ (aq)} + 7H_2O \text{ (l)} = 12H_2 \text{ (g)} + 6CO_2 \text{ (g)} \qquad [1]$$
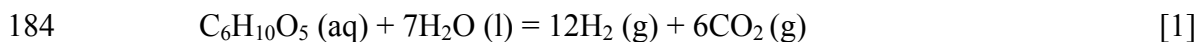
185

186   **Fig. 5b** shows the profiles of H_2 evolution catalyzed by the *in vitro* artificial enzymatic pathway

187   on starch (i.e., 0.1 and 0.4 M glucose equivalents) at 80°C (**Table 1**). The maximum volumetric

188   productivities of H_2 were 360 mmol H_2/L/h with 0.1 M maltodextrin and 530 mmol H_2/L/h with

189   0.4 M maltodextrin, respectively (**Fig. 5b**). When 0.4 M maltodextrin was used~~the substrate~~,

190   more G6P was generated, resulting in higher volumetric productivities (**Fig. 5b**). Maltodextrin is

191   a slowly-utilized substrate, resulting in a 2.5-hour plateau at the maximum volumetric

192   productivity.

193

194   Long-Term H$_2$ Production

195   Long-term enzymatic H$_2$ production is important to demonstrate its feasibility of future scale-up

196   but NAD(P) is infamously unstable, especially at evaluated temperatures [26, 34]. To solve this

197   problem, NAD-conjugated mG6PDH and NAD-conjugated m6PGDH, were constructed by

198   using NAD-poly(ethylene glycol) (PEG)-enzyme conjugates [35, 36]. Specific activities of these two

199   dehydrogenases were not greatly changed by the formation of NAD-PEG-enzyme conjugates

200   (**Fig. S3**). These NAD-PEG-enzyme conjugates exhibited comparable or even better

201   performances for hydrogen generation without addition of free NAD (**Figs. S3&S4**).

202

203   Long-term reaction was conducted by the repeated addition of starch (0.4 M in glucose

204   equivalent) at 80°C with the fifteen hyperthermophilic enzymes including NAD-conjugated

205   mG6PDH and NAD-conjugated m6PGDH (**Table S4**) (**Fig. 6**). The control reaction was carried

206   out by using free NAD$^+$ and two non-conjugated dehydrogenases. The experiment with NAD-

207   dehydrogenase conjugates exhibited the repeated hydrogen peak formations for each substrate

208   addition and its production prolonged for up to nine days, whereas the control reaction stopped

209   producing hydrogen after two days although there were excess substrate and active enzymes

210   (**Fig. 6a**). Approximately 109,000 moles of H$_2$ was produced per 1 mole of the conjugated NAD$^+$

211   at 80°C, while the total turn-over number (TTN) of free NAD$^+$ was approximately 5,700 (**Fig.

212   6b**). The use of conjugated NAD enabled nearly 20-fold improvement in TTN and decreased

213   enzymatic production cost greatly (**Table S3**).

214

215   **Discussion**

216   Three major improvements of this study in comparison of the previous study [12] were 1) a

217   biomimetic NAD-based ETC involving an abiotic electron mediator BV and a novel DI that

218   mimic ferredoxin and FNR, respectively; 2) utilization of the first set of 15 hyperthermophilic

219   enzymes and NAD-conjugated dehydrogenases, allowing production of hydrogen at 80°C for up

220   to nine days; and 3) a BCV-DI facilitating the efficient electron transfer reaction in the

221   conjugate. These improvements were important for (1) achieving the highest production rate of

222   biohydrogen (**Figs. 5 and 6a**), (2) producing hydrogen for nine days at 80^oC (**Fig. 6**), and (3)

223   decreasing the estimated hydrogen production costs by nearly 20-fold by using thermostable

224   enzymes and conjugated NAD rather than NADP used previously (**Table S3**).

225

226   Increasing volumetric productivity of H_2 is one of the most important criteria for distributed

227   ~~green~~ H_2 production because it is closely related with land occupied, hidden cost for energy

228   harvesting, plus equipment size accompanied with capital expenditure [4]. Volumetric productivity

229   of 530 mmol of H_2/L/h is the highest biohydrogen production rate ever reported, equivalent to a

230   glucose utilization rate of 7.95 g/L/h, which is higher than those of typical ethanol yeast

231   fermentations [37]. With a volumetric productivity of >1.0 g H_2/L/h achieved, an anaerobic

232   bioreactor of 62.5 m^3 can produce 1,500 kg H_2 per day. Considering typical sizes for anaerobic

233   bioreactors in beer fermentation and alcohol production, it is very feasible to construct an 80-m^3

234   bioreactor in distributed H_2-refilling stations that can make 1,500 kg H_2 per day. In contrast, the

235   same solar-to-H_2 production capacity plant requires more than 100,000 m^2 of land, assuming a

236   12% solar-energy-to-H_2 efficiency and given an average insolation of 200 W/m^2 for direct water

237   spitting regardless of biological and photochemical ways [17, 38]. Such large land use plus hidden

238   H_2-harvesting costs raises the question whether direct solar water splitting for H_2 production

239   could be widely used [5, 39]. This advanced biological water splitting energized by carbohydrate

240   requires much larger land area than hydrogen production with photoelectrochemical water

241   splitting [5, 6, 8, 10] by considering the land required for plant photosynthesis. Plant photosynthesis

242   has very low solar-energy-to-biomass efficiencies of ~1% for dedicated plants and ~0.2% for the

243   global average [15]. However, the use of natural plant photosynthesis and available carbohydrate as

244   the enriched chemical energy for hydrogen production has two advantages: the abundant

245   renewable biomass (carbohydrate) resource, more than five times of the global human energy

246   consumption; and the available or less-costly infrastructure of carbohydrate processing and

247   distribution.

248

249   After a decade of continuous efforts, more than 1,000-fold increases in volumetric productivity

250   of H_2 from starch has been achieved from 0.48 mmol H_2/L/h [13]. Such dramatic volumetric

251   productivity enhancements are attributed to numerous aspects, including 1) the use of

252   hyperthermophilic enzymes that allow increased reaction temperatures, thereby increasing

253   enzyme activities and decreasing H_2 solubility and H_2 inhibition, 2) the introduction of

254   biomimetic NAD-based ETC to facilitate electron transfer (**Fig. 1b**), 3) the construction of BV-

255   conjugated DI for fast electron transfer (**Fig. 3**), 4) optimization of enzyme ratios by

256   mathematical modeling [11], and 5) the use of highly activity enzyme BioBricks (for example,

257   aldolase [40]). It is anticipated that volumetric productivity of H_2 could be enhanced by another

258   order of magnitude in a few years by 1) developing more efficient enzyme complexes, including

259   SHI and dehydrogenases [41], 2) the use of small and more stable biomimetic coenzymes for better

260   mass transfer [26, 27], 3) the use of enzymes with higher specific activities, for example, the

261   replacement of [NiFe]-hydrogenase SHI with a more active [FeFe]-hydrogenase [42], and 4) the

262   construction of thermostable multiple-cascade enzyme machines such as the Krebs cycle

263   metabolon [43].

264

265   The first thermophilic NAD-based PPP was developed by engineering the cofactor specificity of

266   G6PDH and 6PGDH. Because NROR is not able to efficiently transfer electrons from NADH to

267   BV [29], a new hyperthermophilic DI of *T. maritima* was discovered to implement the first NAD-

268   based biomimetic ETC (**Fig. 1b**) although previously annotated as a putative nitrite reductase

269   subunit. The biomimetic ETC had some notable advantages over the natural ferredoxin-based

270   ETC, including 1) the BV-conjugated DI was thermostable (even at 80°C); 2) both DI and

271   (oxidized) BV are insensitive to O_2, while many ferredoxins and/or FNR are O_2 labile; and 3)

272   BV-conjugated DI may be used for numerous types of hydrogenases, while FNR and ferredoxins

273   have higher selectivity for their interacting partners. In addition, economic analysis suggests that

274   the replacement of NADP with conjugated NAD is the most important cost factor to decrease *in*

275   *vitro* H_2 production costs when hyperthermophilic enzymes were used (**Table S3**) [20]. Also, this

276   NAD-based PPP could also be very useful in *in vivo* synthetic biology projects by balancing

277   coenzyme supply and consumption [44-46].

278

279   There are a few carbon-neutral scenarios for generating kinetic energy on wheels from solar

280   energy (**Fig. 7**). When liquid alcohols are chosen for energy storage compounds, several

281   challenges are low conversion efficiency from CO_2/solar energy regardless of biocatalysts or

282   photocatalysts, high product separation costs, and low energy efficiencies of internal combustion

283   engines [47, 48]. Similarly, direct solar water splitting for hydrogen production plagues from low

284   conversion efficiencies, high harvesting costs for hydrogen, and low storage density of hydrogen

285   [3, 5-7]. Solar cells can address the solar-to-electricity efficiency and energy harvesting, but this

286   system suffer from low electricity storage densities of rechargeable batteries. The use of starch, a

287   natural energy storage compound, which can be isolated from plant seeds or even made from

288   lignocellulosic biomass [49], is an out-of-the-box solution for green hydrogen production and high-

289   density H_2 storage carrier (i.e., up to 14.8% H_2 mass) [12]. However, this advanced biological water

290   splitting approach could have its weaknesses: (1) relatively high production costs (e.g.,10.6-17.7

291   per GJ of hydrogen based on carbohydrate only) mainly due to high prices of carbohydrates (e.g.,

292    $0.18 (future) - $0.30 (current) per kg of carbohydrate) [2]; (2) low energy efficiency solar-energy-

293   to-carbohydrate in plant photosynthesis (e.g., theoretical efficiencies of 4.6-6% for C3 and C4

294   plants, an average efficiency of ~1% for dedicated plants) [15], and (3) large amounts of water

295   consumption and land usage for plant cultivation [15]. Beyond the green hydrogen production, this

296   study implied that the use of renewable carbohydrate as a high-density hydrogen storage

297   compound could address challenges associated with off-board hydrogen storage and costly

298   infrastructure for the hydrogen economy.

299

Conclusions

301   This hydrogen-producing study based on advanced biological water splitting energized by starch

302   featured up to 1,000-fold enhancement in volumetric productivity of hydrogen, achieving a

303   milestone of more than one gram of hydrogen per liter per hour. The use of the first set of 15

304   hyperthermophilic enzymes and two NAD-conjugated dehydrogenases enabled this *in vitro*

305   enzyme cocktail to produce hydrogen for nine days at 80°C without supplementary addition of

306   enzymes and coenzymes. This biological water splitting in darkness could be a promising

307   solution to the distributed production of continuous green H_2 by utilizing the evenly-distributed

308   renewable carbohydrates.

309

310

317

Contributions

319   YZ conceived of the project, oversaw, and coordinated research; EJK and YZ designed

320   experiments; EJK performed experiments; JEK contributed experimental materials; EJK

321   analyzed data; EJK and YZ made figures; and YZ and EJK wrote the paper.

322

Competing financial interests.

324   All authors declare no competing financial interests.

References

325

326   1.   K. Christopher and R. Dimitrios, *Energy Environ. Sci.*, 2012, **5**, 6640-6651.
327   2.   Y.-H. P. Zhang, *Energy Environ. Sci.*, 2009, **2**, 272-282.
328   3.   R. M. Navarro, M. A. Pena and J. L. G. Fierro, *Chem. Rev.*, 2007, **107**, 3952-3991.
329   4.   J. M. Clomburg, A. M. Crumbley and R. Gonzalez, *Science*, 2017, **355**.
330   5.   J. Gu, J. A. Aguiar, S. Ferrere, K. X. Steirer, Y. Yan, C. Xiao, James L. Young, M. Al-
331   Jassim, N. R. Neale and J. A. Turner, *Nat. Energy*, 2017, **2**, 16192.
332   6.   A.-Y. Zhang, W.-Y. Wang, J.-J. Chen, C. Liu, Q.-X. Li, X. Zhang, W.-W. Li, Y. Si and
333   H.-Q. Yu, *Energy Environ. Sci.*, 2018, DOI: 10.1039/C7EE03482B, DOI:
334   10.1039/C1037EE03482B.
335   7.   S. Kosourov, M. Jokel, E.-M. Aro and Y. Allahverdiyeva, *Energy Environ. Sci.*, 2018,
336   DOI: 10.1039/C8EE00054A, DOI: 10.1039/C1038EE00054A.
337   8.   J. H. Kim, J.-W. Jang, Y. H. Jo, F. F. Abdi, Y. H. Lee, R. van de Krol and J. S. Lee, *Nat.*
338   *Commun.*, 2016, **7**, 13380.
339   9.   A. Landman, H. Dotan, G. E. Shter, M. Wullenkord, A. Houaijia, A. Maljusch, G. S.
340   Grader and A. Rothschild, *Nat. Materials*, 2017, **16**, 646-651.
341   10. Y. Yan, R. W. Crisp, J. Gu, B. D. Chernomordik, G. F. Pach, Ashley R. Marshall, J. A.
342   Turner and M. C. Beard, *Nat. Energy*, 2017, **2**, 17052.
343   11. J. A. Rollin, J. Martin del Campo, S. Myung, F. Sun, C. You, A. Bakovic, R. Castro, S. K.
344   Chandrayan, C.-H. Wu, M. W. W. Adams, R. S. Senger and Y.-H. P. Zhang, *Proc. Natl.*
345   *Acad. Sci. USA*, 2015, **112**, 4964-4969.
346   12. J.-E. Kim, E.-J. Kim, H. Chen, C.-H. Wu, M. W. W. Adams and Y.-H. P. Zhang, *Metab.*
347   *Eng.*, 2017, **44**, 246-252.
348   13. Y.-H. P. Zhang, B. R. Evans, J. R. Mielenz, R. C. Hopkins and M. W. W. Adams, *PLoS*
349   *One*, 2007, **2**, e456.
350   14. J. Woodward, M. Orr, K. Cordray and E. Greenbaum, *Nature*, 2000, **405**, 1014-1015.
351   15. Y.-H. P. Zhang, *Energy Sci. Eng.*, 2013, **1**, 27-41.
352   16. S. Rumpel, J. F. Siebel, C. Fares, J. Duan, E. Reijerse, T. Happe, W. Lubitz and M.
353   Winkler, *Energy Environ. Sci.*, 2014, **7**, 3296-3301.
354   17. M. Oey, A. L. Sawyer, I. L. Ross and B. Hankamer, *Plant Biotechnol. J.*, 2016, **14**, 1487-
355   1499.
356   18. A. Veit, M. K. Akhtar, T. Mizutani and P. R. Jones, *Microb. Biotechnol.*, 2008, **1**, 382-
357   394.
358   19. G. J. Schut and M. W. W. Adams, *J. Bacteriol.*, 2009, **191**, 4451-4457.
359   20. Y.-H. P. Zhang, *Biotechnol. Adv.*, 2015, **33**, 1467–1483.
360   21. G. K. Kumaraswamy, T. Guerra, X. Qian, S. Zhang, D. A. Bryant and G. C. Dismukes,
361   *Energy Environm. Sci.*, 2013, **6**, 3722-3731.
362   22. Y.-H. P. Zhang, J. Sun and Y. Ma, *J. Ind. Microbiol. Biotechnol.*, 2017, **44**, 773-784.
363   23. S. K. Chandrayan, C.-H. Wu, P. M. McTernan and M. W. W. Adams, *Protein Expr.*
364   *Purif.*, 2015, **107**, 90-94.
365   24. A. Liese and L. Hilterhaus, *Chem. Soc. Rev.*, 2013, **42**, 6236-6249.
366   25. H. Chen, Z. G. Zhu, R. Huang and Y.-H. Zhang, *Sci. Rep.*, 2016, **6**, 36311.
367   26. C. E. Paul, I. W. C. E. Arends and F. Hollmann, *ACS Catal.*, 2014, **4**, 788-797.
368   27. C. You, R. Huang, X. Wei, Z. Zhu and Y.-H. P. Zhang, *Syn. Syst. Biotechnol.*, 2017, **2**,
369   208-218.
370   28. R. Huang, H. Chen, C. Zhong, J. E. Kim and Y.-H. P. Zhang, *Sci. Rep.*, 2016, **6**, 32644.

371   29.   E.-J. Kim, M. Adams, C.-H. Wu and Y. H. P. Zhang, *Chemistry*, 2016, **22**, 16047–16051.
372   30.   J. Collins, T. Zhang, S. Huston, F. Sun, Y. H. P. Zhang and J. Fu, *PLoS ONE*, 2016, **11**,
373   e0154865.
374   31.   Z. G. Zhu and Y.-H. P. Zhang, *Metab. Eng.*, 2017, **39**, 110-116.
375   32.   P. H. Ninh, K. Honda, T. Sakai, K. Okano and H. Ohtake, *Biotechnol. Bioeng.*, 2015, **112**,
376   189-196.
377   33.   C. You, T. Shi, Y. Li, P. Han, X. Zhou and Y.-H. P. Zhang, *Biotechnol. Bioeng.*, 2017,
378   **114**, 1855-1864.
379   34.   K. Honda, N. Hara, M. Cheng, A. Nakamura, K. Mandai, K. Okano and H. Ohtake,
380   *Metab. Eng.*, 2016, **35**, 114-120.
381   35.   T. Kishimoto, M. Itami, T. Yomo, I. Urabe, Y. Yamada and H. Okada, *J. Ferm. Bioeng.*,
382   1991, **71**, 447-449.
383   36.   A. Nakamura, I. Urabe and H. Okada, *J. Biol. Chem.*, 1986, **261**, 16792-16794.
384   37.   S.-J. Ha, J. M. Galazka, S. Rin Kim, J.-H. Choi, X. Yang, J.-H. Seo, N. Louise Glass, J.
385   H. D. Cate and Y.-S. Jin, *Proc. Natl. Acad. Sci. USA*, 2011, **108**, 504-509.
386   38.   P. J. L. Williams and L. M. L. Laurens, *Energy Environ. Sci.*, 2010, **3**, 554-590.
387   39.   K. Kalyanasundaram and M. Graetzel, *Curr. Opin. Biotechnol.*, 2010, **21**, 298-310.
388   40.   C. You and Y. H. P. Zhang, *ACS Syn. Biol.*, 2014, **3**, 380-386.
389   41.   P. C. Jordan, D. P. Patterson, K. N. Saboda, E. J. Edwards, H. M. Miettinen, G. Basu, M.
390   C. Thielges and T. Douglas, *Nat. Chem.*, 2016, **8**, 179-185.
391   42.   N. Khanna and P. Lindblad, *Int. J. Mol. Sci.*, 2015, **16**, 10537.
392   43.   F. Wu and S. Minteer, *Angew. Chem. Int. Ed.*, 2014, **127**, 1871–1874.
393   44.   W. D. Huang and Y.-H. P. Zhang, *Energy Environ. Sci.*, 2011, **4**, 784-792.
394   45.   S. Brinkmann-Chen, T. Flock, J. K. B. Cahn, C. D. Snow, E. M. Brustad, J. A. McIntosh,
395   P. Meinhold, L. Zhang and F. H. Arnold, *Proc. Natl. Acad. Sci. U.S.A.*, 2013, **110**,
396   10946-10951.
397   46.   K. Qiao, T. M. Wasylenko, K. Zhou, P. Xu and G. Stephanopoulos, *Nat. Biotechnol.*,
398   2017, **35**, 173-177.
399   47.   Gurudayal, J. Bullock, D. F. Sranko, C. M. Towle, Y. Lum, M. Hettick, M. C. Scott, A.
400   Javey and J. Ager, *Energy & Environmental Science*, 2017, **10**, 2222-2230.
401   48.   Y. H. P. Zhang, *Proc. Biochem.*, 2011, **46**, 2091-2110.
402   49.   C. You, H. Chen, S. Myung, N. Sathitsuksanoh, H. Ma, X.-Z. Zhang, J. Li and Y. H. P.
403   Zhang, *Proc. Natl. Acad. Sci. USA*, 2013, **110**, 7182.
404   50.   W.-D. Huang and Y.-H. P. Zhang, *PLOS ONE*, 2011, **6**, e22113.

405

406 **Figure Legends**

407 **Figure 1.** Scheme of the direct NADP-based electron transfer from NADPH to H_2 *via* soluble

408 hydrogenase I (SHI), glucose 6-phosphate dehydrogenase (G6PDH), and 6-phosphogluconate

409 dehydrogenase (6PGDH) (a); scheme of the NAD-based ETC from NADH to H_2 comprised of

410 NAD-dependent glucose 6-phosphate dehydrogenase (mG6PDH), NAD-dependent 6-

411 phosphogluconate dehydrogenase (m6PGDH), 6-phosphogluconolactonase (6PGL), diaphorase

412 (DI), and BV (b); scheme of an alternative NAD-based ETC from NADH to H_2 comprised of

413 mG6PDH, m6PGDH, 6PGL, and BCV-DI (c); and scheme of the NAD-based ETC from NADH

414 to H_2 comprised of NAD-conjugated mG6PDH, NAD-conjugated m6PGDH, 6PGL, and BCV-

415 DI (d).

416

417 **Figure 2**. Coenzyme engineering of G6PDH with a coenzyme preference from $NADP^+$ to NAD^+.

418 Simulated docking structure between G6PDH and $NADP^+$ (a) and redox-dye-based screening

419 plates for three mutant libraries (i.e., S33, A64 and R65/T66) and positive clones identified on

420 screening plates followed by their combination – the best mutant mG6PDH – S33E/R65M/T66S

421 (b).

422

423 **Figure 3.** Simulated docking structure between NROR and $NADP^+$ (a), simulated docking

424 structure of DI with NAD^+ and FAD (b), comparisons of transhydrogenase activities of NROR

425 and DI from NAD(P)H to the oxidized electron mediator benzyl viologen (BV^{2+}) at $50^{\circ}C$ (c), and

426 profiles of H_2 evolution from 0.1 M G6P at $50^{\circ}C$ (d). The enzyme cocktails were (1) mG6PDH +

427 SHI; (2) mG6PDH + SHI + DI (0.1 mM) + BV (0.6 mM); and (3) mG6PDH + SHI + BCV-DI

428 (0.1 mM).

429

430 **Figure 4**. Preparation steps for BCV-DI (a) and the NAD-dependent H_2 evolution profiles (b)

431 from 0.2 M G6P at $80^{\circ}C$ *via* the enzyme cocktails (i.e., mG6PDH + SHI + BCV-DI; mG6PDH +

432 m6PGDH + SHI + BCV-DI; and mG6PDH + m6PGDH + 6PGL + SHI + BCV-DI). 25 μM

433 BCV-DI (1 g/L) was added for all reactions.

434

435 **Figure 5**. Scheme of *in vitro* NAD-based synthetic enzymatic pathway for *in vitro* H_2 production

436 energized by starch (a) and NAD-dependent H_2 evolution profiles (b) from starch (0.1 M and 0.4

437   M in glucose equivalent, respectively) at 80°C *via* the entire pathway containing BCV-DI (**Table**

438   **1**).

439

440   **Figure 6**. Long-term H_2 evolution profiles (a) and their TTN values (b) from the repeated adding

441   of starch (i.e., 0.4 M in glucose equivalent) at 80°C *via* the entire pathway containing NAD-

442   conjugated mG6PDH and NAD-conjugated m6PGDH (**Table S4**) in comparison to the case with

443   non-conjugated NAD. The experiments were carried out in 100 mM HEPES buffer (pH 7.5) at

444   80°C, as described in **Figure 5**.

445

446   **Figure 7**. Comparison of different carbon-neutral scenarios from solar energy to mechanic

447   energy on wheels through (1) liquid solar fuels (e.g., alcohols) followed by internal combustion

448   engines; (2) starch (a natural solar fuel) followed by water splitting (this study) followed by

449   hydrogen storage tank, proton exchange membrane fuel cell (PEMFC), and electric motor (EM),

450   (3) direct water splitting for H_2 generation followed by a hydrogen storage tank, PEMFC, and

451   EM; and (4) electricity generation *via* solar cells followed by rechargeable battery and EM. More

452   details of energy efficiency analysis are available elsewhere [50].

Table 1. Enzymes used for hydrogen generation from starch.

Enzyme (Abbreviation)	E.C. #	Gene Source	Sp. Act. at 50°C (U/mg)	Enzyme Loading (U/mL)	Reference
α-glucan phosphorylase (αGP)	2.4.1.1	*Thermotoga maritima*	20^1	5	[33]
Phosphoglucomutase (PGM)	5.4.2.2	*Thermococcus kodakarensis*	100^1	5	[33]
NAD-dependent G6P dehydrogenase (mG6PDH)	1.1.1.49	*T. maritima*	12^2	5	This study
6-phosphogluconolactonase (6PGL)	3.1.1.31	*T. maritima*	230^3	5	[31]
NAD-dependent 6PG dehydrogenase (m6PGDH)	1.1.1.44	*T. maritima*	35^1	5	[25]
Ribose 5-phosphate isomerase (RPI)	5.3.1.6	*T. maritima*	300	2	[31]
Ribulose 5-phosphate 3-epimerase (RuPE)	5.1.3.1	*T. maritima*	66	2	[31]
Transketolase (TK)	2.2.1.1	*Thermus thermophilus*	5.3	2	[31]
Transaldolase (TAL)	2.2.1.2	*T. maritima*	3.9	2	[31]
Triose-phosphate isomerase (TIM)	5.3.1.1	*T. thermophilus*	450	1	[40]
Aldolase (ALD)	4.1.2.13	*T. thermophilus*	16	1.5	[40]
Fructose 1,6-bisphosphatase (FBP)	3.1.3.11	*T. maritima*	6	2	[31]
Phosphoglucose isomerase (PGI)	5.3.1.9	*T. thermophilus*	190^1	2	[32]
BCV-DI	1.18.1.4	*T. maritima*	20^4	20	This study
[NiFe]-Hydrogenase (SHI)	1.12.1.3	*Pyrococcus furiosus*	121^5	300	[23]

^{1}Specific activity was measured at 70°C

^{2}Specific activity was measured at 80°C

^{3}Specific activity was measured at 23°C

^{4}Specific activity of BCV-DI (1 g/L of BCV-DI contains 0.15 mM BV)

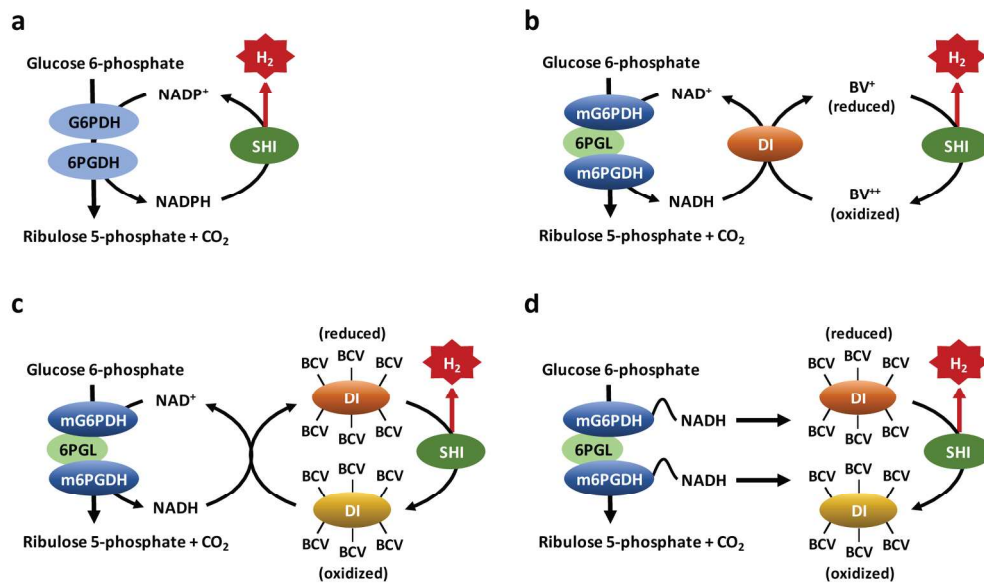^{5}Specific activity of SHI was 121 U/mg based on reduced methyl viologen at 80°C [23].

Figure 1. Scheme of the direct NADP-based electron transfer from NADPH to H2 via soluble hydrogenase I (SHI), glucose 6-phosphate dehydrogenase (G6PDH), and 6-phosphogluconate dehydrogenase (6PGDH) (a); scheme of the NAD-based ETC from NADH to H2 comprised of NAD-dependent glucose 6-phosphate dehydrogenase (mG6PDH), NAD-dependent 6-phosphogluconate dehydrogenase (m6PGDH), 6-phosphogluconolactonase (6PGL), diaphorase (DI), and BV (b); scheme of an alternative NAD-based ETC from NADH to H2 comprised of mG6PDH, m6PGDH, 6PGL, and BCV-DI (c); and scheme of the NAD-based ETC from NADH to H2 comprised of NAD-conjugated mG6PDH, NAD-conjugated m6PGDH, 6PGL, and BCV-DI (d).

181x108mm (300 x 300 DPI)
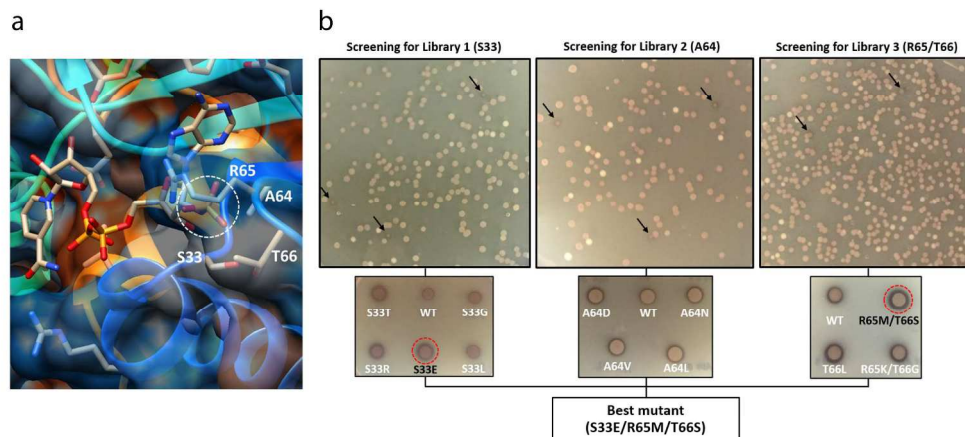
Figure 2. Coenzyme engineering of G6PDH with a coenzyme preference from NADP+ to NAD+. Simulated docking structure between G6PDH and NADP+ (a) and redox-dye-based screening plates for three mutant libraries (i.e., S33, A64 and R65/T66) and positive clones identified on screening plates followed by their combination – the best mutant mG6PDH – S33E/R65M/T66S (b).
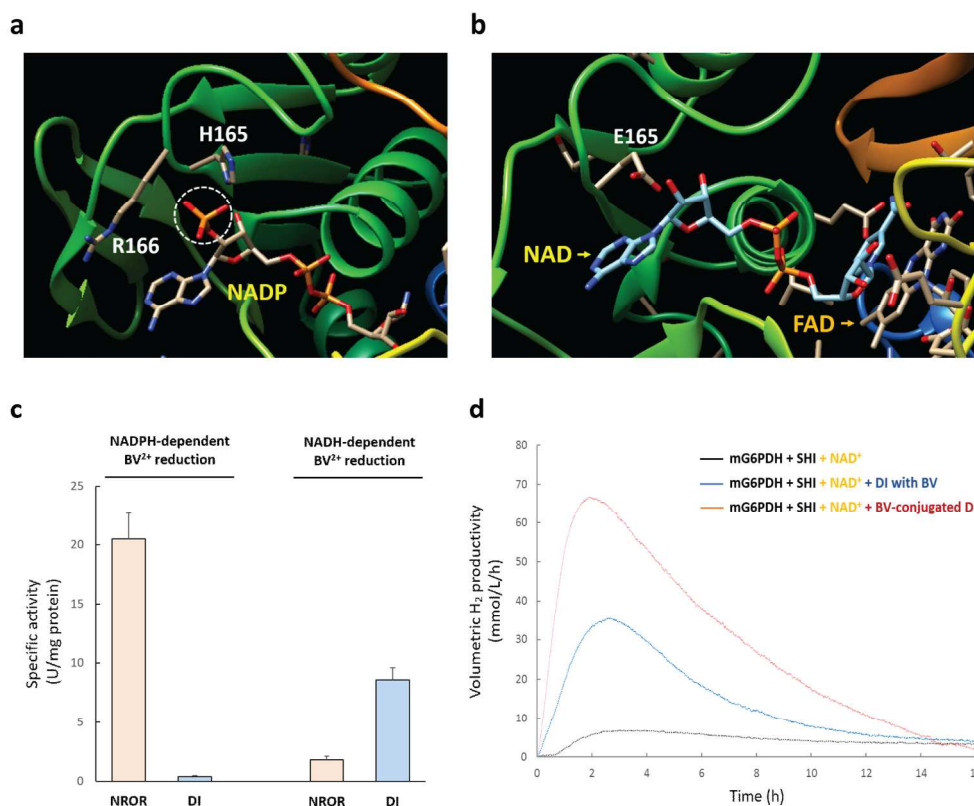
254x190mm (300 x 300 DPI)

Figure 3. Simulated docking structure between NROR and NADP+ (a), simulated docking structure of DI with NAD+ and FAD (b), comparisons of transhydrogenase activities of NROR and DI from NAD(P)H to the oxidized electron mediator benzyl viologen (BV2+) at 50oC (c), and profiles of H2 evolution from 0.1 M G6P at 50oC (d). The enzyme cocktails were (1) mG6PDH + SHI; (2) mG6PDH + SHI + DI (0.1 mM) + BV (0.6 mM); and (3) mG6PDH + SHI + BCV-DI (0.1 mM).

181x149mm (300 x 300 DPI)
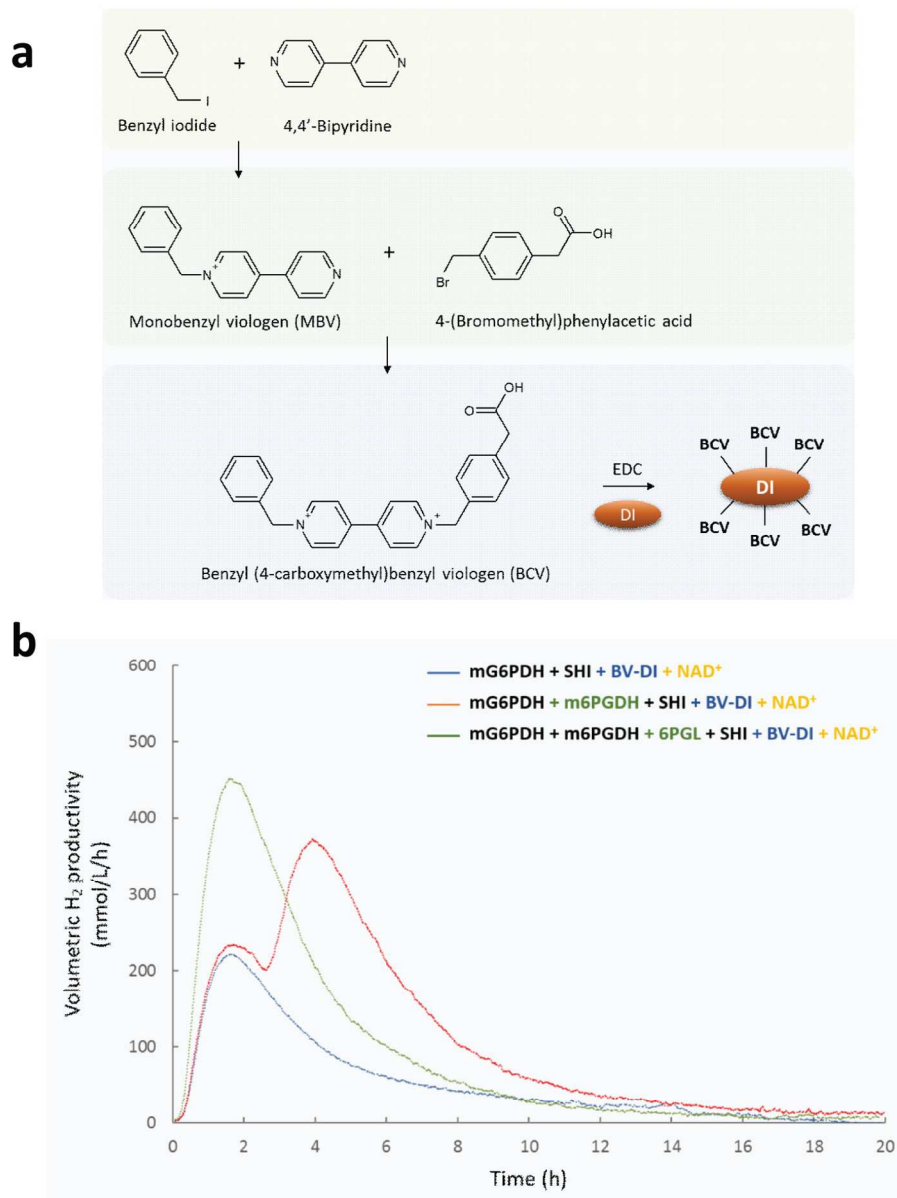
Figure 4. Preparation steps for BCV-DI (a) and the NAD-dependent H2 evolution profiles (b) from 0.2 M G6P at 80oC via the enzyme cocktails (i.e., mG6PDH + SHI + BCV-DI; mG6PDH + m6PGDH + SHI + BCV-DI; and mG6PDH + m6PGDH + 6PGL + SHI + BCV-DI). 25 µM BCV-DI (1 g/L) was added for all reactions.
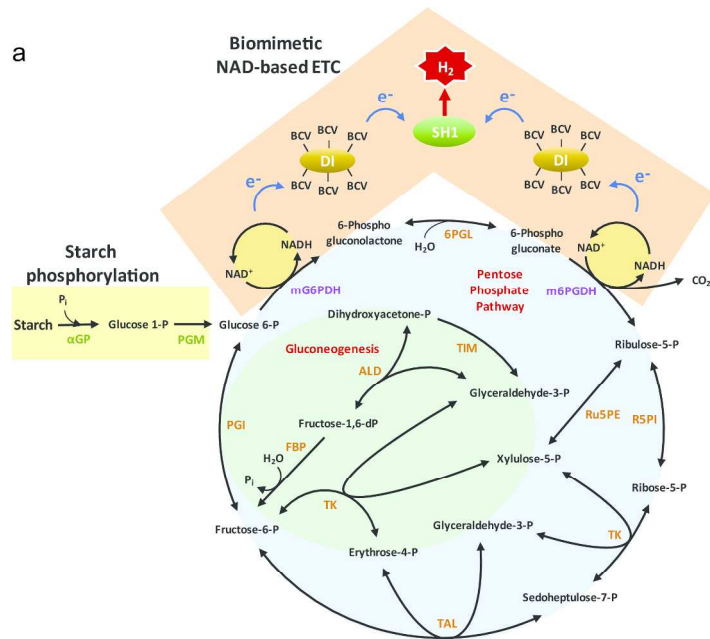
127x163mm (300 x 300 DPI)

Figure 5a. Scheme of in vitro NAD-based synthetic enzymatic pathway for in vitro H2 production energized by starch (a) and NAD-dependent H2 evolution profiles (b) from starch (0.1 M and 0.4 M in glucose equivalent, respectively) at 80oC via the entire pathway containing BCV-DI (Table 1).
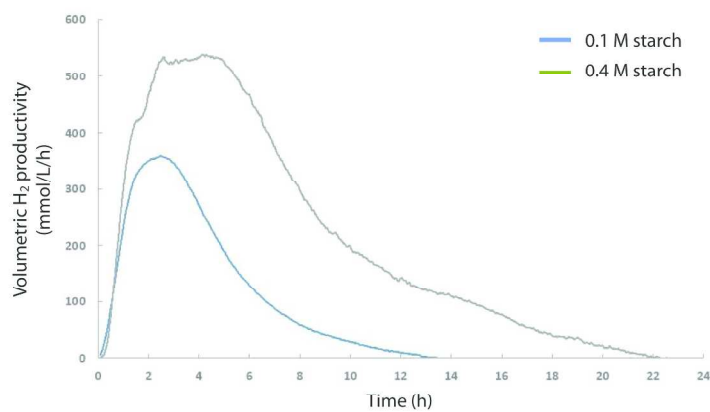
245x161mm (300 x 300 DPI)

Figure 5b. Scheme of in vitro NAD-based synthetic enzymatic pathway for in vitro H2 production energized by starch (a) and NAD-dependent H2 evolution profiles (b) from starch (0.1 M and 0.4 M in glucose equivalent, respectively) at 80oC via the entire pathway containing BCV-DI (Table 1).
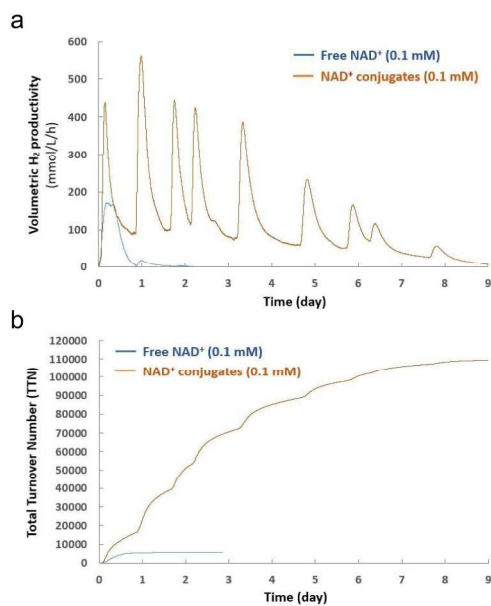
254x190mm (300 x 300 DPI)

Figure 6. Long-term H2 evolution profiles (a) and their TTN values (b) from the repeated adding of starch (i.e., 0.4 M in glucose equivalent) at 80oC via the entire pathway containing NAD-conjugated mG6PDH and NAD-conjugated m6PGDH (Table S4) in comparison to the case with non-conjugated NAD. The experiments were carried out in 100 mM HEPES buffer (pH 7.5) at 80oC, as described in Figure 5.
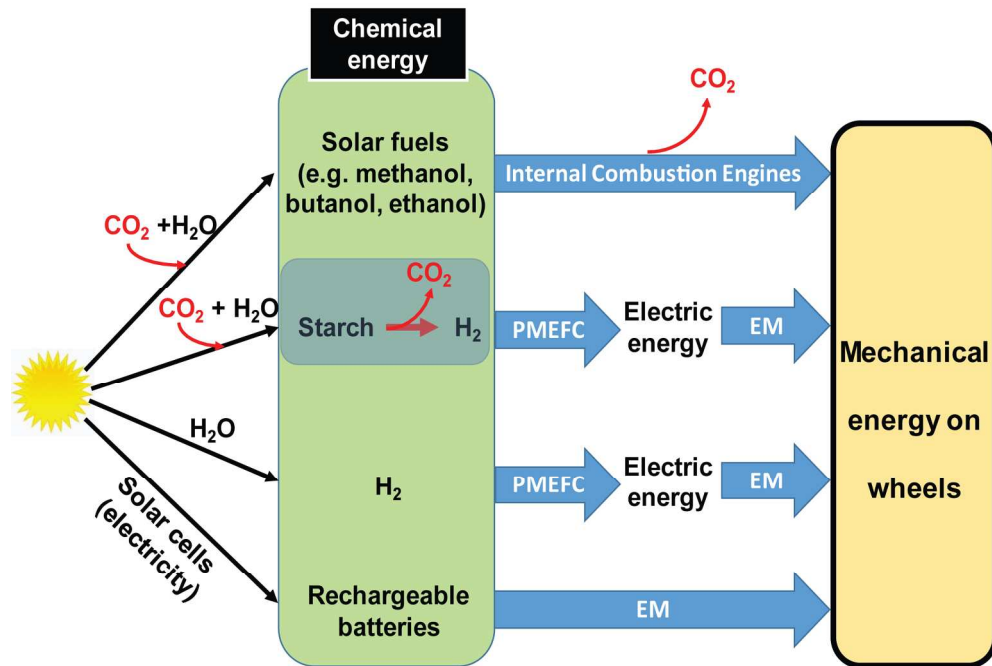
254x190mm (300 x 300 DPI)

Figure 7. Comparison of different carbon-neutral scenarios from solar energy to mechanic energy on wheels through (1) liquid solar fuels (e.g., alcohols) followed by internal combustion engines; (2) starch (a natural solar fuel) followed by water splitting (this study) followed by hydrogen storage tank, proton exchange membrane fuel cell (PEMFC), and electric motor (EM), (3) direct water splitting for H2 generation followed by a hydrogen storage tank, PEMFC, and EM; and (4) electricity generation via solar cells followed by rechargeable battery and EM. More details of energy efficiency analysis are available elsewhere 48.

175x116mm (300 x 300 DPI)

Table of Content

TITLE: Ultra-Rapid Rates of Water Splitting for Biohydrogen Gas Production through *in vitro* Artificial Enzymatic Pathways

Authors: Eui-Jin Kim, Jae-Eung Kim, and Yi-Heng P. Job Zhang

Ultra-rapid biohydrogen is produced from water splitting energized by a natural energy storage compound starch with the artificial enzymatic biosystem.